ACS Sustainable Chemistry & Engineering

pubs.acs.org/journal/ascecg

Research Article

Functionalized Lignin Nanoparticles for Sustainable Rubber Compounds

Mattia Carnevale,[†] Federica Ferruti,*[,†] Luciano Tadiello, Silvia Guerra, Luca Giannini, Marco Orlandi, and Luca Zoia

Cite This: https://doi.org/10.1021/acssuschemeng.5c12029

Read Online

ACCESS | Metrics & More | Article Recommendations | Supporting Information

ABSTRACT: The transition toward sustainable tire manufacturing requires renewable alternatives to fossil-derived reinforcing fillers, such as carbon black (CB). Lignin is a promising biobased candidate; however, its application in rubber is limited by poor dispersion and weak interfacial compatibility. In this work, lignin nanoparticles (LNPs) with tunable size were prepared via a solvent-shifting process and incorporated into natural rubber (NR) using an optimized latex-based predispersion strategy. The nanostructured lignin exhibited uniform morphology and enabled improved dispersion and filler−matrix interfacial area compared to bulk lignin, resulting in enhanced mechanical reinforcement. To further promote interfacial interactions, LNPs were surface-functionalized with cystamine, a bioderived diamine containing a disulfide moiety active during vulcanization. Surface modification was confirmed by spectroscopic and elemental analyses, and the curing curve revealed accelerated vulcanization. Rubber compounds in which CB was partially replaced by cystamine-functionalized LNPs displayed tensile and dynamic mechanical properties comparable to carbon-black-filled references while maintaining low hysteresis. This study demonstrates that combining lignin nanostructuring with targeted surface functionalization enables effective partial substitution of CB, offering a scalable pathway toward more sustainable rubber reinforcement systems.

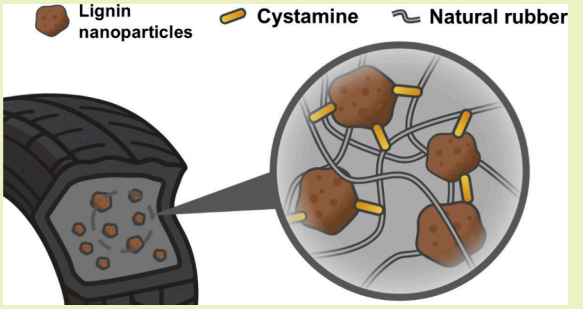

KEYWORDS: *lignin modification, lignin nanoparticles, natural rubber, elastomers, biobased filler*

1. INTRODUCTION

The global tire industry faces increasing pressure to adopt sustainable practices, driven by regulatory demands, consumer awareness, and the urgent need to reduce greenhouse gas emissions and reliance on finite fossil resources. In this context, the development of renewable alternatives to fossil-derived materials has emerged as a key research priority, particularly in the design of reinforcing fillers for rubber compounds.[1] Traditionally, carbon black (CB) has been the dominant reinforcing agent due to its excellent mechanical reinforcement properties. However, CB production is energy-intensive and heavily dependent on petroleum feedstocks, contributing to carbon emissions and environmental pollution. The transition to biobased reinforcing fillers thus represents a critical step in advancing the sustainability profile of elastomeric composites for tires.

Lignin, a major component of lignocellulosic biomass, is the second most abundant natural polymer on the earth. Among all of the different types of lignins, kraft lignin is the most widely available as a low-cost byproduct from the pulping and paper industry.[2] Despite these benefits, the direct use of lignin in rubber composites has been limited due to the poor compatibility between lignin and nonpolar rubber matrixes, often leading to agglomeration and weak filler−matrix interactions, resulting in a compromised mechanical performance.[3]

A conventional strategy to incorporate lignin into rubber systems includes the direct mixing of dry lignin with the rubber compound, resulting in inadequate dispersion of the filler in the matrix and degradation of the mechanical performance of the composite. Later, a coprecipitation technique was developed, including the coagulation of a predispersion obtained by adding an alkaline lignin solution to natural rubber (NR) latex, which resulted in a better dispersion of the filler in the elastomer and evidenced improved mechanical properties.[3] Despite the advancements offered by the latter process, both methods proved inadequate to finely tune the filler size, morphology, and interfacial behavior, which are critical parameters for achieving reinforcement comparable to that of CB. In the context of particle size control, nanostructuring has emerged as an effective strategy to enhance

Received: November 6, 2025
Revised: March 2, 2026
Accepted: March 3, 2026

performance. Nanometric scale is associated with a higher surface area when compared to its microscale counterpart, guaranteeing a high number of interactions between the filler and the matrix in which the former is dispersed.[4,5] Several methods have been reported for the synthesis of lignin nanoparticles (LNPs), ranging from mechanical grinding to ultrasonication to aerosol flow processes.[6−8] Among these methods, solvent exchange is particularly attractive for its ability to produce spherical particles with controlled size distribution and its potential scalability.[9−12]

Although LNPs have been integrated in composite materials,[13] their incorporation into rubber compounds remains limited, possibly due to the lack of effective and scalable strategies for incorporating LNPs into rubber matrixes while preserving particle integrity and achieving homogeneous dispersion. Latex-based predispersion approaches have been proposed as a promising route to overcome these challenges because they enable intimate mixing at the colloidal level prior to drying and compounding.[14]

Controlling the lignin particle size prior to compounding also provides opportunities for targeted compatibilization at the filler−matrix interface. Conventional lignin modifications typically involve bulk functionalization, which is often inefficient and reagent-demanding. In contrast, surface-specific modification of nanoscale lignin enables efficient functionalization while minimizing chemical usage, directly supporting sustainable material development.[15] Literature reports various approaches for LNP surface modification through the adsorption of cationic species such as PDADMAC, chitosan, proteins, and cationic lignin, exploiting Coulombic and hydrogen-bonding interactions with lignin's carboxylic acid groups.[17−20] Surface functionalization is a well-established strategy in silica-filled rubber systems, where sulfides-containing silane coupling agents are used to enhance dispersion and form covalent filler−rubber linkages during vulcanization.[16] In this regard, cystamine, a diamine derived from cysteine and containing a disulfide linkage, has been shown to enhance silica−rubber interactions and has been proposed as a more sustainable alternative to conventional silane coupling agents.[17,18]

This work explores the preparation, functionalization, and incorporation of cystamine-modified LNPs into NR-based nanocomposites. By combining nanoscale particle engineering, targeted surface modification, and scalable latex-assisted processing routes, the study aims to enhance filler dispersion, improve interfacial bonding, and reduce reliance on fossil-derived reinforcing agents. This approach intends to improve the mechanical performance while aligning with the goals of sustainability and reduced environmental impact in tire manufacturing.

2. RESULTS AND DISCUSSION

2.1. LNPs and Cystamine Functionalization

2.1.1. LNPs Preparation and Characterization. The complete dissolution of lignin in the selected solvent mixture is a critical prerequisite for obtaining well-defined LNPs because incomplete dissolution can lead to residual coarse particles and broad size distributions.[19] Previous studies have screened various solvents for lignin processing;[12,20,21] however, for industrial scalability and sustainability considerations, certain options were excluded. Toxic solvents such as tetrahydrofuran and those with high boiling points, including dimethyl sulfoxide (DMSO), γ-valerolactone, and ethylene glycol, were avoided due to environmental and energy-intensive recovery concerns. Furthermore, nonbiobased solvents were disregarded to align with the renewable-material focus of this work. A binary mixture of acetone and water was ultimately selected.[22] Acetone offers multiple advantages: its volatility facilitates complete recovery without azeotrope formation, it is potentially producible from biobased routes via microbial fermentation, and prior studies reported that acetone−water mixtures yield smaller particles compared to ethanol−water systems.[23] Lignin solubility was assessed using various acetone−water mixtures, with a 3:1 ratio providing the best results, as illustrated in Figure S1.

LNPs were synthesized via solvent shifting using a fixed antisolvent-to-solvent ratio of 10, with KL concentrations (C_i) in acetone−water [3:1 (w/w)] ranging from 20 to 180 g·kg^{-1}.

Dynamic light scattering (DLS) measurements provided the hydrodynamic diameter (D_h) and dispersity ($Đ$) of the resulting particles (Figure 1). The LNPs exhibited sizes

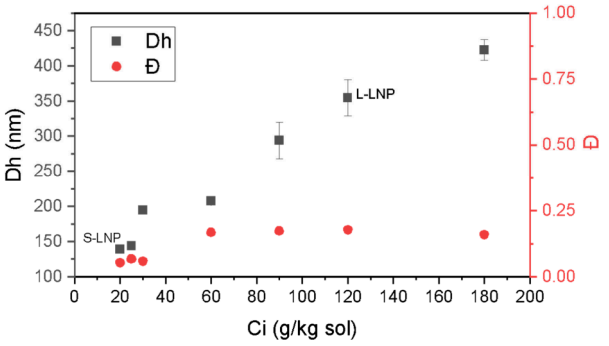

Figure 1. DLS measurements of D_h and $Đ$ of LNPs by varying C_i. Error bars can be smaller than the symbols.

between 150 and 450 nm with a clear correlation between C_i and D_h, enabling size tuning through a single variable. This phenomenon is consistent with previously reported self-assembly behavior: upon rapid introduction into the antisolvent, lignin molecules aggregate with nearby molecules, and higher solute concentrations favor the formation of larger particles.[24] Particles prepared at low C_i displayed narrow distributions ($Đ$ < 0.1), whereas increasing C_i not only enlarged the particle size but also broadened $Đ$. Above 180 g·kg^{-1}, the colloidal stability diminished, leading to flocculation and sedimentation. Notably, smaller LNPs (∼50 nm) could be obtained at very low concentrations, but their practical application was limited by insufficient solid content in the resulting dispersions. For subsequent rubber compounding, filler powders or concentrated suspensions (10−20 wt %) are required; thus, the prepared LNP suspensions necessitated postsynthesis concentration steps.

Two representative samples were selected for comprehensive characterization, with a particular focus on morphology and surface features: small lignin nanoparticles (S-LNPs) and large lignin nanoparticles (L-LNPs), obtained from initial solution concentrations of C_i of 20 and 120 g·kg^{-1}, respectively. Scanning electron microscopy (SEM) confirmed the spherical morphology and smooth surfaces of both materials (Figure 2). S-LNPs displayed a uniform population around 100 nm, whereas L-LNPs showed a broader size distribution (100−400 nm) and some agglomeration, attributed to lignin's intermolecular interactions during sample

https://doi.org/10.1021/acssuschemeng.5c12029
ACS Sustainable Chem. Eng. XXXX, XXX, XXX−XXX

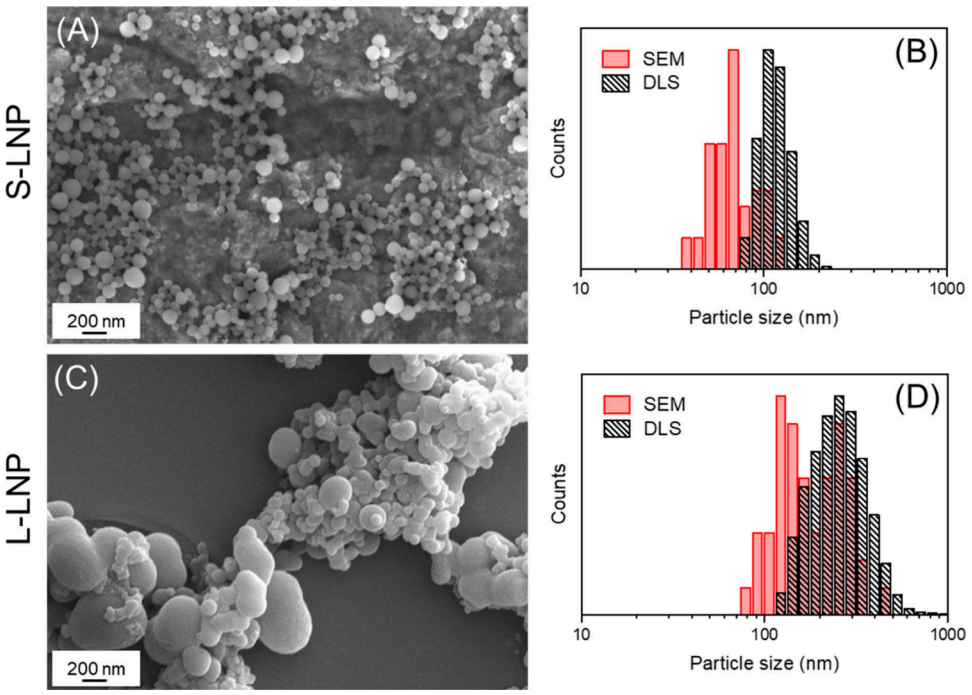

Figure 2. SEM micrographs of (A) S-LNP and (C) L-LNP and their particle size distribution histograms (B and D, respectively). Particle size distribution histograms obtained with a population of 50 LNPs per sample for SEM images and as an average of the counts of three measurements for DLS.

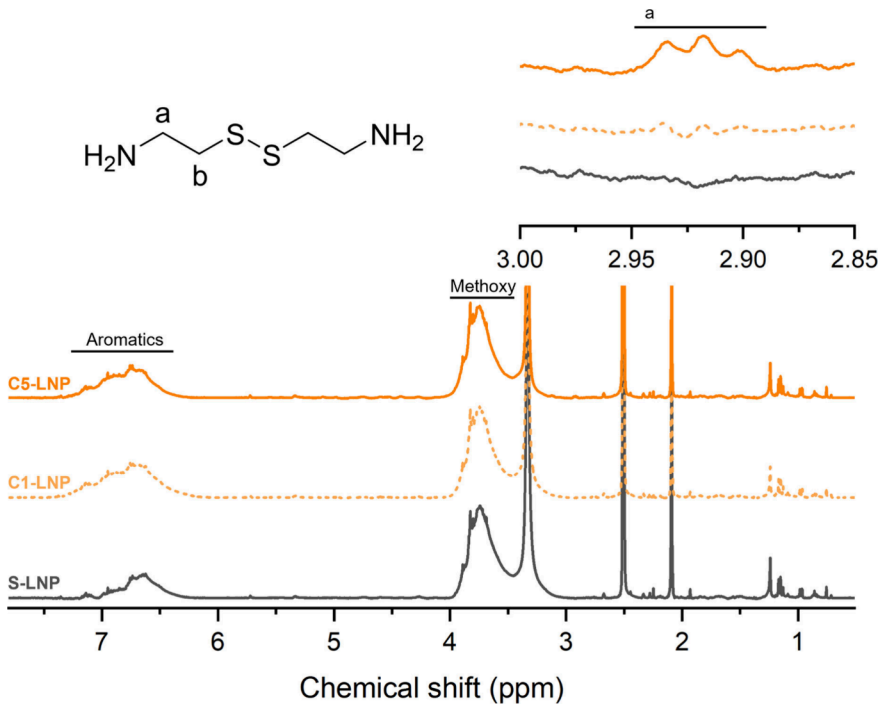

Figure 3. ^{1}H NMR spectroscopy of functionalized LNPs at two different loadings in DMSO, C1-LNP, and C5-LNP. S-LNP is reported for reference; intensities are normalized with the methoxy group peak at 3.75 ppm.

drying after deposition on sample holders (stubs). Compared to the DLS data, the particle size revealed by SEM showed the expected shrinkage associated with the air drying faced by LNPs during preparation of the microscopy specimen.[25]

Nitrogen adsorption−desorption isotherms revealed the absence of micro- or mesopores, with only small hysteresis at relative pressures above 0.95, suggesting the presence of macropores associated with interparticle voids. The calculated Brunauer−Emmett−Teller (BET) surface areas were determined as 11.05 ± 0.05 $m^2 \cdot g^{-1}$ for S-LNPs and 4.18 ± 0.03 $m^2 \cdot g^{-1}$ for L-LNPs, consistent with their respective particle sizes.

2.1.2. Surface Functionalization of LNPs with Cystamine. As reported in the literature, LNPs can be surface-specifically functionalized by polyelectrolyte adsorption.[12]

https://doi.org/10.1021/acssuschemeng.5c12029
ACS Sustainable Chem. Eng. XXXX, XXX, XXX−XXX

Surface modification of LNPs was explored via ionic interactions with cystamine, a diamine that contains a disulfide bridge. KL contains carboxylic acid groups ($pK_a \sim 4-5$) and phenolic groups ($pK_a \sim 9-11$).[25] Complete deprotonation of carboxylic acids and partial deprotonation of phenolic groups are ensured by cystamine, which has a conjugate acid pK_a of 9−10. Considering an estimated number of carboxylic acid groups per gram of kraft lignin ranging from 0.5 to 0.9 mmol·g^{-1}, as characterized in a previous work,[15] a series of experiments with cystamine loadings from 0 to 0.7 mmol·g^{-1} per gram of LNP were conducted using S-LNPs as the substrate, in order to maximize the effect of functionalization in association with the largest surface area of the lignin particles included in the study.

A pool of complementary analyses allowed investigation of the functionalization of LNPs with cystamine.

The presence of disulfide bonds was qualitatively confirmed using a 2-nitro-5-thiobenzoate (NTB) assay,[26] which could supply a qualitative evaluation and not a quantification due to the solubility limitation of our system, with the assay being developed for soluble analytes and LNPs being a suspension (Tables S1−S3). Elemental analysis corroborated increased sulfur and nitrogen contents upon functionalization with cystamine, offering the nitrogen content a more accurate estimation of the effective cystamine loading than the sulfur content, because kraft lignin already contains a nonnegligible amount of sulfur (Table S4). ^{1}H NMR spectra (Figure 3) showed an increase in the intensity of peak a proportionally to the cystamine content, further supporting a successful modification, despite the low intensity of the signal, which was expected on the basis of the extent of the cystamine loading, which was limited by the number of lignin's ionizable groups prone to making an ionic pair with cystamine's amino groups.

The system was designed to ensure a surface functionalization of LNPs with cystamine through ionic interaction, which was supported by the correlation of the cystamine loading with dimensions and surface charge. DLS and ζ-potential measurements revealed that, by increasing the cystamine loading, dimensions increased and the ζ potential grew less negative (Figure 4). In particular, low cystamine loadings (<0.2 mmol·g^{-1}) induced only small particle size increases and maintained colloidal stability, with observations after 36 h confirming negligible postfunctionalization aggregation and sedimentation. Above the aforementioned loading threshold, D_h increased significantly, indicating aggregation, and the ζ potential approached neutrality, consistent with surface charge neutralization from ionic pairing.

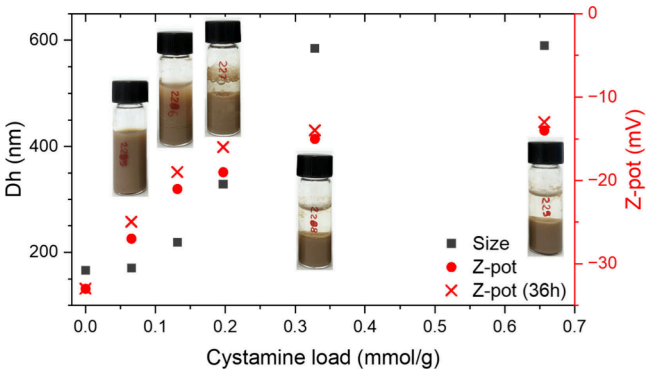

Figure 4. Measurement of D_h (black squares) by DLS and of the ζ potential (Z-pot; red circles and crosses) for surface-functionalized LNPs by varying the loading of cystamine. Z-pot measurements were performed after functionalization (circles) and 36 h after formulation (crosses). Digital images of the suspensions after 12 h from formulation are reported at their corresponding loading values.

Two functionalized LNPs were selected for further study: C1-LNPs (a cystamine content of 0.07 mmol·g^{-1}, approximately equal to 1 wt %) and C5-LNP (a cystamine content of 0.33 mmol·g^{-1}, approximately equal to 5 wt %), representing loadings below and above the size-variational threshold of 0.2 mmol·g^{-1}, respectively.

2.2. Elastomeric Compounds Including LNPs as Filler

2.2.1. Preparation of NR−Lignin Masterbatch. LNP predispersions in NRs, termed masterbatches or MB in the following, were prepared by two different methods. The first approach consisted of adding freeze-dried LNPs in an internal mixer to NR, after 30 in. of premastication, expecting to retain the filler size. Captivated by studies reporting a more homogeneous dispersion of the filler inside the matrix, a NR latex predispersion was prepared. Thus, the second process to include lignin in the elastomeric matrix consisted of mixing intimately LNPs and NR as water-based colloids and subsequently solidifying the mixture to a dry masterbatch of lignin in NR.[3] The resulting R-MB, S-MB, and L-MB included kraft lignin as a reference, S-LNPs ($D_h \sim 100$ nm), and L-LNPs ($D_h \sim 100-400$ nm), respectively. The second method of mixing lignin and NR, before predispersions were prepared, required concentration of the LNP suspensions by partial water evaporation. DLS analysis before and after water evaporation confirmed that the particle size was largely retained; however, the high solid content promoted the formation of micrometric aggregates. These were subsequently broken down using a homogenizer to ensure redispersion. Following the mixing of concentrated LNP suspensions with a NR latex, the removal of water was required in order to isolate the MB. A previously reported method presented the coagulation of lignin and NR suspensions by acidic precipitation, followed by the filtration of excess water, washing with fresh water until reaching nearly neutral pH, and drying.[3] In light of chemical economy and scalability, in the present work, MBs were prepared by mixing LNPs suspensions and a NR latex and drying them while heating under stirring, in order to avoid sedimentation of LNPs and to obtain homogeneous suspensions.[27]

In order to envision the dispersion and morphology of the filler in the matrix, SEM samples were prepared by cryogenically fracturing MBs in liquid nitrogen and exposing their surfaces to analysis (Figure 5). The reference MB prepared with kraft lignin (R-MB) displayed embedded micrometric particles, consistent with prior studies.[3] In contrast, both S-MB and L-MB, containing LNPs, exhibited only submicrometric particles, appearing either as isolated entities or as small aggregates. This morphology demonstrates that LNPs retain their nanostructure during processing and disperse more uniformly than unmodified kraft lignin, resulting in a nanocomposite with a higher filler−matrix interfacial area.

To evaluate whether ammonia, used as a stabilizer in a NR latex, influenced the LNP morphology, the particle sizes observed in the SEM were compared with previously reported data. Size distributions showed slight reductions compared to initial values, attributed to partial emersion of LNPs embedded

https://doi.org/10.1021/acssuschemeng.5c12029
ACS Sustainable Chem. Eng. XXXX, XXX, XXX−XXX

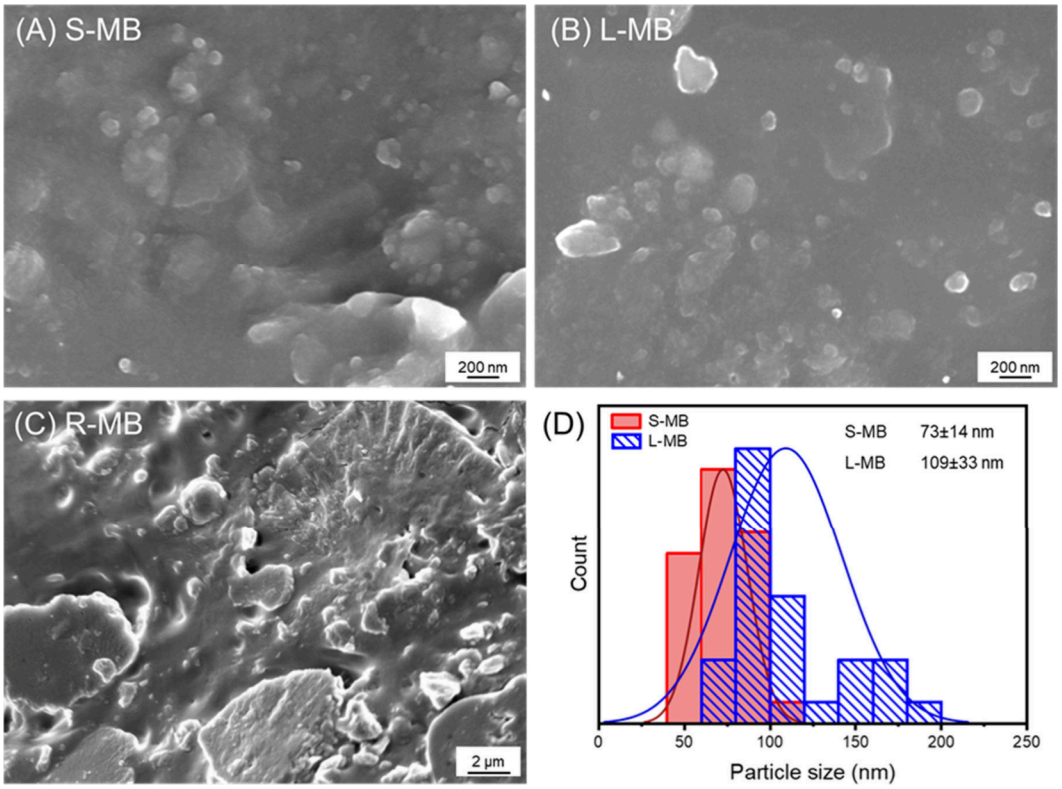

Figure 5. SEM micrographs of fractures of frozen LNP masterbatches (A) S-MB, (B) L-MB, and (C) R-MB. (D) Particle size distribution histograms (30 measures per sample).

in the NR matrix during fracture, resulting in an underestimation of their real size rather than to the partial degradation of particles.

To further investigate the mechanism of composite formation, a droplet of the NR latex/LNP mixture was rapidly quenched in deionized water and imaged via SEM (Figure S2). While cryogenically fractured MB imaging showed no significant aggregation, this quenching experiment revealed an LNP aggregate surrounded by NR latex microparticles. This suggests a degree of interfacial compatibility between LNP surfaces and NR particles during early stages of mixing, a phenomenon that may facilitate uniform dispersion upon drying.

Fourier transform infrared (FT-IR) spectra of MBs (Figure 6) revealed characteristic bands of NR: 3050−2800 cm^{-1} (C−H stretching of alkanes and alkenes), 1450 and 1390 cm^{-1} ($-CH_3$ and $-CH_2-$ stretching), and 850−800 cm^{-1} (C═C bending overlapping with aliphatic rocking modes). The incorporation of lignin, whether as unmodified kraft lignin (in R-MB) or as LNPs (in S-MB and L-MB), did not significantly alter these spectral features. Peaks characteristic of lignin were also present: 3300−3000 cm^{-1} (O−H stretching), 1500 cm^{-1} (aromatic C−C stretching), and 1300−1000 cm^{-1} (aliphatic C−O stretching).

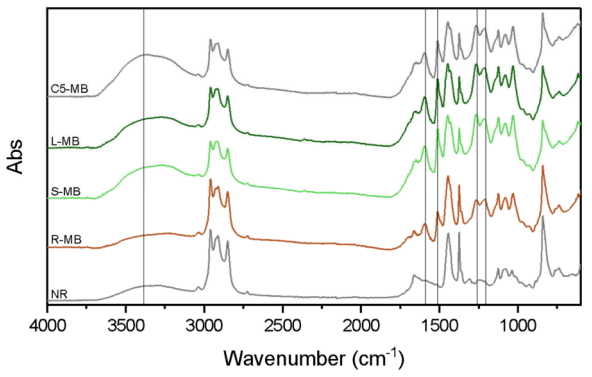

Figure 6. FT-IR/ATR spectra of NR masterbatches filled with 100 phr of kraft lignin, S-LNP, L-LNP, and C5-LNP (R-MB, S-MB, L-MB, and C5-MB, respectively) and of unfilled NR for reference.

The spectrum of cystamine-functionalized LNP composites (C5-MB) exhibited a slight shift in the broad 3600−3000 cm^{-1} band toward higher wavenumbers, indicative of N−H stretching and confirming the successful incorporation of amine groups from cystamine. Another MB containing a lower loading of cystamine (C1-MB) was prepared and analyzed, but its spectrum is not reported because it was comparable to that of C5-MB.

2.2.2. Full Replacement of CB in Rubber Compounds. The reinforcing capability of LNPs in NR compounds was assessed by formulating model composites containing 50 phr of a single filler and other ingredients including antioxidants and vulcanizing agents. Compounds 50R, 50S, and 50L were prepared using predispersed R-MB, S-MB, and L-MB, respectively. More explicitly, 50R, 50S, and 50L were compounds prepared from lignin/NR masterbatches and included KL, S-LNPs, and L-LNPs as reinforcing fillers. For comparison, compounds 50Rdry and 50Sdry were produced by mixing freeze-dried lignin or S-LNP powders into NR via premastication in an internal mixer, followed by the addition of the other ingredients. A reference compound, 50CB, was prepared with 50 phr of CB. Among the various commercial CB grades, N326 was selected as a reference due to its

https://doi.org/10.1021/acssuschemeng.5c12029
ACS Sustainable Chem. Eng. XXXX, XXX, XXX−XXX

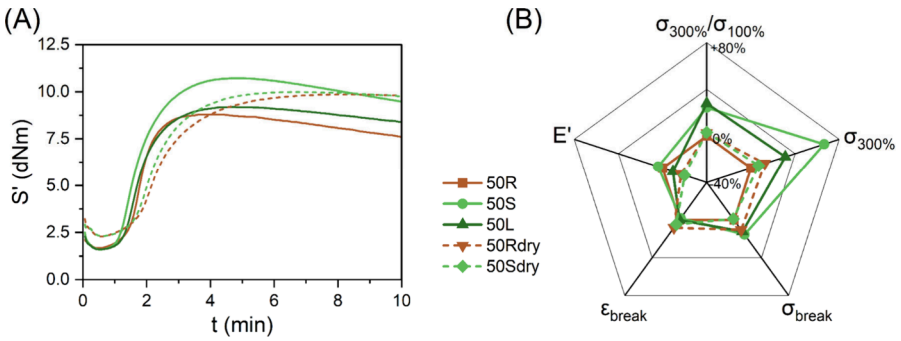

Figure 7. (A) Vulcanization curves of various NR compounds filled with 50 phr of S-LNP (50S predispersed in NR and 50Sdry added as powder), L-LNP (50L), and suitable references. The torque (S') was measured over time while curing at 170 °C. (B) Static and dynamic mechanical properties measured with tensile tests of various NR compounds filled with 50 phr S-LNP (50S predispersed in NR and 50Sdry added as powder), L-LNP (50L), and suitable references.

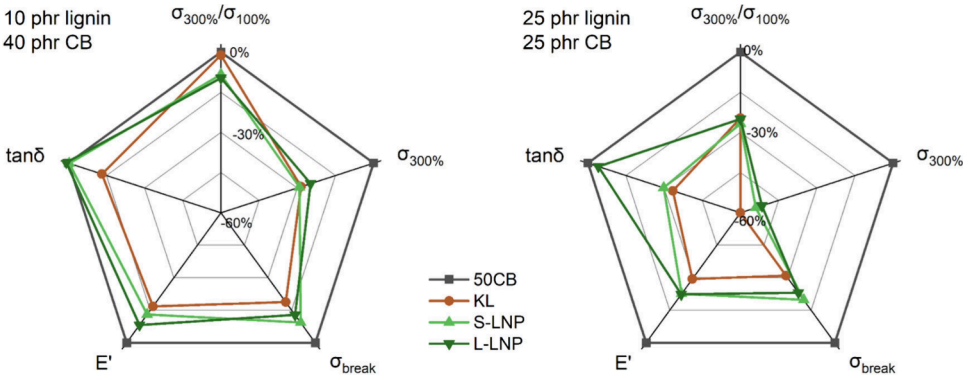

Figure 8. Static ($\sigma_{300\%}/\sigma_{100\%}$, σ_{break}, and ε_{break}) and dynamic (E' and tan δ at 70 °C/10 Hz) properties expressed as a percentage variation from the reference (50CB) of NR compounds filled with ref, S-LNP, and L-LNP.

properties: moderate surface area (~80 $m^2 \cdot g^{-1}$), low structure (low aggregation), and particle sizes in the 30−40 nm range. This CB grade is widely used in tire components such as carcasses, belts, and undertreads, offering a low modulus but high tensile strength and elongation.

The prepared compounds, along with different lignin grades and NR, included other ingredients typical for elastomeric composites for tire applications, including antioxidants, vulcanization agents, etc., as detailed in the section devoted to materials and methods. A simplified composition of the compounds, in terms of the filler content and process of inclusion of the filler in the matrix, is reported in Table S5.

The vulcanization curves of the compounds were analyzed via rubber process analysis (RPA). Torque (S') evolution during curing is shown in Figure 7A, and the value of the main parameters can be found in Table S5. At the onset, low torque values correspond to a reduction in viscosity due to the elevated temperature, reaching a minimum torque (ML). Compounds made with predispersions generally exhibited lower ML values, likely due to weaker filler−filler interactions. As cross-linking progressed, torque increased, peaking at maximum torque (MH). The curing behavior of composites where lignin was predispersed in NR was similar to that of the reference 50CB compound, with t90 values only slightly higher. Mild reversion was observed in all samples, reducing the final torque and marginally deteriorating the mechanical properties. Among lignin-filled samples, 50S achieved the highest MH values (excluding 50CB), followed by 50L and 50R, indicating that smaller LNPs provide better reinforcement due to their higher surface area. A similar trend was noted when 50Sdry and 50Rdry were compared; however, dry-mixed compounds consistently exhibited lower MH and slower curing, which could be attributed to poorer dispersion.

Tensile testing results (Table S6) confirmed that lignin-filled compounds were generally softer than 50CB, with lower moduli and tensile strengths. However, S-MB-based compounds demonstrated significant reinforcement relative to R-MB, as evidenced by manifold parameters: the stress at 300% strain, which was incremented by 66% compared to R-MB; the modulus ratio, which was incremented by 23% compared to R-MB; the stress at break, which was incremented by 15% compared to R-MB.

Ultimate elongation remained comparable, indicating improved reinforcement without compromising the elasticity. Dynamic moduli by compression tests show a trend similar to static tensile moduli, with the modulus depending mostly on the amount of CB. Dynamic hysteresis is higher for compounds filled with S nanoparticles than with L nanoparticles, correlating with a higher contact area between filler and rubber. The trend of dynamic hysteresis agrees with the classical theory of reinforcement of fillers noncovalently bound to rubber, according to which the filler−rubber interface dynamic is dominated by stick-and-slip phenomena that contribute to energy dissipation.[28]

2.2.3. Replacement of CB in Rubber Compounds. Model compounds were prepared including lignin of different grades (unmodified kraft lignin, S-LNPs, and L-LNPs) in partial substitution of CB in order to assess the use of LNP in technical rubber compounds, considering a compound reinforced by 50 phr of CB (50CB) as our technological

https://doi.org/10.1021/acssuschemeng.5c12029
ACS Sustainable Chem. Eng. XXXX, XXX, XXX−XXX

reference and target. One-to-one substitution of CB was achieved in compounds including unmodified kraft lignin (10R-40CB and 25R-25CB), S-LNPs (10S-40CB and 25S-25CB), and L-LNPs (10L-40CB and 25L-25CB). For a complete list of the model compounds prepared and their relative filler content, refer to Table S7.

The results of mechanical characterizations of the prepared samples are visualized in Figure 8 and summarized in Table S8. The vulcanization curve revealed t90 values comparable for all of the compounds. Both the maximum torque (MH) and minimum torque (ML) decreased as the lignin content increased, reaching their lowest values in fully CB-substituted compounds (50R, 50S, and 50L).

Tensile testing confirmed the reinforcing effect of the dual-filler system. Stress values at 100% and 300% deformation and ultimate stress values were remarkably lower for lignin-only compounds (50R, 50S, and 50L) than for the 50CB benchmark. However, compounds with 40 phr of CB in combination with all lignins achieved a modulus ratio comparable to that of 50CB, indicating similar reinforcement. Their ultimate strength ($\sigma_{@break}$) also matched the reference while maintaining higher elongation at break ($\varepsilon_{@break}$), a typical feature of lignin-containing rubbers, which found its momentum in the case of LNPs-containing compounds.

Dynamic mechanical analysis revealed a relatively high Payne effect for lignin-containing compounds, indicating the formation of strong filler networks (Table S8). Hysteresis values remained below those of 50CB, suggesting a reduction in rolling resistance, which was particularly appealing when the lignin content increased.

The particle size significantly influenced the compound behavior. At high CB levels (40 phr), L-LNPs provided slightly better mechanical properties than S-LNPs, while the ultimate tensile strengths remained similar. At lower CB levels, S-LNPs yielded better reinforcement and higher ultimate strength than L-LNPs and unmodified KL. These findings indicate synergistic interactions between CB and LNPs, which can be tuned through both the filler ratio and nanoparticle size.

To further investigate the filler synergies, the work of adhesion (W) between CB and lignin in NR was calculated as a theoretical index of interaction between CB N326 (referred to as 1 in the following formulas) and lignin of different grades (KL or LNPs, referred to as 2 in the following formulas) in NR (referred to as 3 in the following formulas).

The solid surface energy of each filler was calculated according to the Owens−Wendt equation (eq 1) from data reported in the literature identifying the dispersive γ_i^d and γ_j^d and polar γ_i^p and γ_j^p contributions to surface tensions for each component, i and j, of the interphase.[29]

$$W_{ij} = 2\sqrt{\gamma_i^d \gamma_j^d} + 2\sqrt{\gamma_i^p \gamma_j^p} \quad (1)$$

The work of adhesion is the work required to separate two phases from each other, and it is related to the interfacial energy between the two phases.[30] When the two phases are separated, the interphase between them, in this case the interphase 1−2 between CB and lignin, is disrupted and new interphases, in this case 1−3 and 2−3 (CB−NR and lignin−NR, respectively), are formed. This phenomenon is taken into consideration in eq 2, which allowed one to calculate W between CB and lignin in NR:

$$W_{132} = W_{12} + W_{33} - W_{13} - W_{23} \quad (2)$$

The calculated parameter W_{132} quantifies the compatibility between two fillers (1 and 2) in a matrix (3).

The positive W values (Table 1) obtained for both bulk lignin and LNPs paired with CB in NR indicate thermodynamic compatibility, suggesting a synergistic interaction and dispersion of the fillers in the matrix rather than segregated filler domains and independent networks. This calculation is consistent with the tendency of lignin to enhance CB dispersion at low loadings reported in the literature.[31−33] A higher W_{132} value when using LNPs, in comparison with bulk lignin, aligns with the enhanced reinforcement performance experimentally observed, proving the role of the nanometric size in improving the dispersion of the fillers.

Table 1. Dispersive (γ^d) and Polar (γ^p) Contributions of the Surface Energy of CB, KL, LNP and NR as Reported in the Literature[29] and Calculated Work of Adhesion (W) of Filler Pairs (CB/KL and CB/LNP) in a Third Medium (NR)

component (i)	γ^d (mJ·m^{-2})	γ^p (mJ·m^{-2})	$W_{CB/NR/lignin}$ (mJ·m^{-2})
CB N326	26.4	0.8	
KL	45.8	10.5	1.85
LNP	42.3	11.4	2.40
NR	35.0	0.12	

Experimental results show that the partial substitution of CB with both bulk lignin and LNPs reduces reinforcement; nonetheless, it offers clear sustainability benefits. The most encouraging results were found when CB was replaced with LNPs, enabling a 20−25% reduction in CB with only a modest decrease (∼10%) in the ultimate strength. In order to develop more sustainable-by-design rubber compounds while pursuing technological competitiveness, a lignin-based filler size in the nanometric range alone is not sufficient. Therefore, a combination of nanosize and surface functionalization was explored with the expectations of increased filler−matrix compatibility resulting in mechanical reinforcement of the composite.

2.3. Elastomeric Compounds Including Cystamine-Functionalized LNPs

Morphological modification of lignin alone was insufficient to preserve reinforcement, highlighting the need for further strategies, such as surface functionalization or compatibilizers, to strengthen filler−matrix interactions, further increase the level of CB replacement, and unlock higher biofiller loadings.

NR model compounds were prepared using cystamine-functionalized S-LNPs in partial replacement of CB. C1-LNPs and C5-LNPs, containing 1 and 5 wt % of cystamine, respectively, were predispersed in NR for the preparation of the corresponding masterbatches C1-MB and C5-MB. The specific filler loadings are summarized in the first section of Table S9. In this study, the reference compounds included CB and the nonfunctionalized S-LNPs as reinforcing fillers.

Vulcanization curves (Figure 9 and Table S9) revealed that incorporating functionalized LNPs accelerated the curing process relative to unmodified S-LNPs. This acceleration increased with the cystamine content, as shown by the decrease in optimum curing times (t90) for the series 25S-25CB, 25C1-25CB, and 25C5-25CB. Functionalized samples also displayed reduced minimum and maximum torque, particularly for C1-LNP formulations (25C1-25CB and 10C1-40CB). Previous studies on amine-modified silica nanoparticles attribute similar effects to the catalytic action

https://doi.org/10.1021/acssuschemeng.5c12029
ACS Sustainable Chem. Eng. XXXX, XXX, XXX−XXX

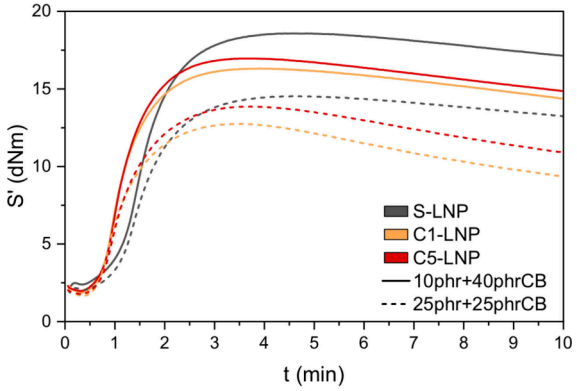

Figure 9. Vulcanization curve of various NR compounds filled with C1-MB and C5-MB at two different loading levels and suitable references (S-MB). Changes in S' are measured over time during curing at 170 °C.

of amino groups during cross-linking, explaining the faster curing observed here.[34] Comparable trends are also seen with disulfide or tetrasulfide silane modifications, where both curing acceleration and reduced filler−filler networking occur, resulting in lower ML and MH values.[35,36]

Static and dynamic mechanical tests (Figure 10 and Table S9) demonstrated how functionalization influenced reinforcement. At low strain levels during dynamic compression, functionalized LNPs slightly decreased the compression modulus (E') by about 5%. The hysteresis (tan δ) increased more notably for C5-LNP than for C1-LNP. Due to variations in stiffness, direct comparisons with nonfunctionalized references require caution.

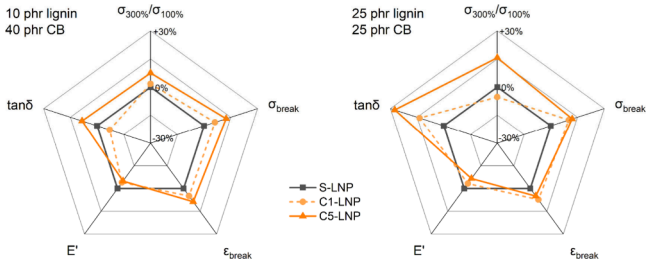

Figure 10. Static ($\sigma_{300\%}/\sigma_{100\%}$, σ_{break}, and ε_{break}) and dynamic (E' and tan δ at 70 °C/10 Hz) properties expressed as a percentage variation from the reference (S-LNP) of NR compounds filled with C1-MB and C5-MB.

At higher strains (static tensile tests), cystamine-functionalized LNPs provided clear reinforcement benefits. C5-LNP compounds exhibited an increased $\sigma_{300\%}/\sigma_{100\%}$ ratio, which could be interpreted as a product of enhanced dispersion of the filler,[37] and augmented tensile strength, with stress at break increasing by roughly 12% compared to that of nonfunctionalized analogues, which could be considered as indirect evidence of a higher content of cross-linking sulfur functionalities, as observed in comparable systems including sulfide-containing organosilanes compatibilizing silica.[38−40] C1-LNPs also improved tensile properties with respect to S-LNPs but to a lesser extent than C5-LNPs. Remarkably, in cystamine-containing systems, elongation at break increased by 5−10%, indicating that reinforcement did not compromise elasticity.

Cystamine functionalization proved particularly effective in enhancing filler dispersion during mixing, mirroring the behavior of disulfide-modified silicas. The most promising formulation, 10C5-40CB, matched or exceeded the tensile performance of the reference 50CB compound while maintaining favorable viscoelastic properties, suggesting a good balance between reinforcement and rolling resistance.

3. CONCLUSIONS

This work demonstrated the successful synthesis and application of cystamine-functionalized LNPs in NR composites. LNPs were produced via solvent shifting, where the particle size was controlled primarily by the initial lignin concentration. Predispersions prepared via a novel drying method enabled high loading (50 wt %) and maintained nanoparticle morphology, enabling for the industry to prepare technical compounds with a high lignin content.

Hybrid LNP/CB systems showed that partial CB replacement with LNPs could maintain mechanical properties while reducing the CB content. Functionalization with cystamine further improved the curing parameters, filler−filler interactions, and tensile properties. However, lignin's intrinsic softness compared to rigid fillers like CB or silica remains a challenge. Enhancing the LNP stiffness is a key target for future work to achieve superior reinforcement.

4. MATERIALS AND METHODS

4.1. Materials

Softwood kraft lignin (BioPiva 100, UPM, Finland) was used to prepare the lignin nanoparticles (LNPs). The lignin (KL) contained 65 wt % dry content and was dried under vacuum at 65 °C before use. Acetone (98%) and cystamine dihydrochloride (96%) were obtained from Merck (Germany).

Stabilized natural rubber (NR) latex with a high ammonia content (NR latex, Von Bundit Co., Thailand) and 60 wt % solid content was used to produce lignin−NR predispersions. Additional raw materials included natural rubber SIR20 (Aneka Bumi Pratama, Indonesia), carbon black N326 (Cabot Corporation, USA), oil-extended sulfur oleate 66% (Crystex OT 33, Eastman, USA), zinc oxide (ZnO, Zincol Ossidi, Italy), stearic acid (SA, Sogis, Italy), Rhenogran TBBS-80 (Lanxess Group, Germany), and *N*-1,3-dimethylbutyl-*N*′-phenyl-*p*-phenylenediamine (6PPD, Flexsys, USA).

4.2. Preparation of LNPs by Antisolvent Precipitation

KL was dissolved in an acetone−water mixture and stirred for 3 h at room temperature in a sealed container to minimize solvent evaporation. The solution was filtered through a sintered glass filter (size 1) to remove residual fibrous material and then rapidly poured into deionized water (antisolvent) under vigorous stirring using a piston pump at 100 mL·min^{-1}. Acetone was removed from the resulting colloidal suspension via rotary evaporation under reduced pressure or by slow evaporation under ambient conditions. The effects of the initial lignin solid content (g of KL per kg of solvent) and solvent/antisolvent ratio on particle formation were investigated.

4.3. Functionalization of LNPs with Cystamine

LNP surface functionalization with cystamine was performed via ionic interactions. Cystamine dihydrochloride was added directly to the LNP suspension in stoichiometric amounts, and the mixture was stirred overnight. For characterization, functionalized nanoparticles were centrifuged and washed twice with deionized water.

4.4. Preparation of Lignin−NR Masterbatches

Predispersions (masterbatches, MBs) of lignin in NR were produced using a codrying technique in which water was removed from lignin−latex mixtures. Lignin (either as a LNP suspension or dissolved lignin for reference) was incorporated into a NR latex at a fixed 7.7 wt %

https://doi.org/10.1021/acssuschemeng.5c12029
ACS Sustainable Chem. Eng. XXXX, XXX, XXX−XXX

solids ratio (equivalent to 1 g of solids per 12 mL of water). LNP suspensions were concentrated to this ratio prior to mixing. The suspensions were added dropwise to a NR latex (60 wt % solids) under vigorous stirring, covered, and homogenized for 30 min. The mixture was then uncovered and heated at 75 °C until dry (overnight). The dried material was cut into small pieces and mixed at 100 °C for 5 min using a Brabender mixer (50 mL chamber, open to release residual water).

Masterbatches containing unmodified LNPs (S-LNP and L-LNP) and cystamine-functionalized LNPs (C1-LNP and C5-LNP) were prepared with a 100 phr loading (50 wt % lignin and 50 wt % NR) and labeled S-MB, L-MB, C1-MB, and C5-MB, respectively. A reference masterbatch (R-MB) was prepared using lignin dissolved in alkaline water (pH 10, adjusted with ammonium hydroxide).

4.5. Rubber Compounding

Lignin-filled NR compounds were produced as model elastomeric materials using a Brabender twin-screw mixer (50 mL chamber). The process involved a first stage of mixing of non-temperature-sensitive ingredients at 120 °C and 60 rpm, followed by the addition of vulcanizing agents at 80 °C and 50 rpm. All formulations contained 100 phr NR (neat or as MB), 2 phr 6PPD, 4 phr ZnO, 2 phr SA, 1.8 phr TBBS, and 4 phr sulfur (67%).

4.6. Characterization Techniques

4.6.1. FT-IR/Attenuated Total Reflectance (ATR) Spectroscopy. Spectra were acquired using a Nicolet iS10 ATR spectrometer (Thermo Scientific) with 32 scans per sample over 4000−600 cm^{-1} at 1 cm^{-1} resolution.

4.6.2. Elemental Analysis. Elemental analysis (C, N, and S) was performed using a Vario microcube (Elementar).

4.6.3. NMR Spectroscopy. Samples (50 mg) were dissolved in 750 μL of DMSO-d_6 and analyzed on a Bruker Avance 500 MHz spectrometer (48K scans for ^{1}H).

4.6.4. Dynamic Light Scattering (DLS). The hydrodynamic diameters (D_h) of LNPs were determined using a ZetaSizer Nano ZS (Malvern) with a 633 nm He−Ne laser at a 173° scattering angle (298 K). Measurements were performed in triplicate using disposable cuvettes; water properties (RI = 1.33; viscosity = 0.8929 cP) were assumed.

4.6.5. Scanning Electron Microscopy (SEM). LNPs were spin-coated on silica wafers or mounted on aluminum stubs with carbon tape. Masterbatches were cryofractured in liquid nitrogen, mounted, sputter-coated with gold, and imaged with a Zeiss Gemini 500 microscope using secondary and in-lens detectors.

4.7. Surface Area Analysis

Specific surface areas were measured by N_2 physisorption (Quantachrome Autosorb-1, Anton-Paar) using the BET and *t*-plot methods. LNPs were freeze-dried and degassed at 80 °C overnight.

4.8. Vulcanization and Dynamic Mechanical Analysis (DMA)

The rheological properties were studied with a RPA 2000 rubber process analyzer (Alpha Technologies). Vulcanization was analyzed at 170 °C (1.6 Hz, 0.5°) for 15 min. DMA was performed on cured samples via a strain sweep (0.1−10%) at 70 °C and 10 Hz.

4.9. Tensile Testing

Stress−strain behavior was evaluated with a Zwick/Roell machine, following ISO 37 and UNI 6065 standards. Compounds were conditioned 24 h, sheeted (8 mm thick), and cured at 170 °C (4.3 bar, 10 min). Dumbbell specimens were die-cut; tensile properties (modulus at 10−300% strain, tensile strength, and elongation at break) were determined from three replicates, and median values were reported.

4.10. Compression Testing

Cylindrical specimens (1.8 mm × 1.2 mm ⌀) were tested in compression at varying temperatures (23, 70, and 100 °C) and frequencies (1, 10, and 100 Hz) under 7.5% strain and 20% precompression. The storage modulus (E'), loss modulus (E''), and tan δ were obtained.

■ ASSOCIATED CONTENT

Supporting Information

The Supporting Information is available free of charge at https://pubs.acs.org/doi/10.1021/acssuschemeng.5c12029.

Detailed description and data on the following topics: optimization of conditions for the dissolution of kraft lignin, NTB assay, elemental analysis, SEM images of lignin−rubber masterbatches, and tables reporting data from static and dynamic mechanical characterization of rubber compounds (PDF)

■ AUTHOR INFORMATION

Corresponding Author

Federica Ferruti − *Corimav-Pirelli, Department of Materials Science, University of Milano−Bicocca, 20125 Milan, Italy;* orcid.org/0000-0002-1104-8005; Email: f.ferruti@campus.unimib.it

Authors

Mattia Carnevale − *Corimav-Pirelli, Department of Materials Science, University of Milano−Bicocca, 20125 Milan, Italy;* orcid.org/0000-0003-0944-1702

Luciano Tadiello − *Pirelli Tyre S.p.A., 20126 Milan, Italy*

Silvia Guerra − *Pirelli Tyre S.p.A., 20126 Milan, Italy*

Luca Giannini − *Pirelli Tyre S.p.A., 20126 Milan, Italy;* orcid.org/0000-0002-5842-6384

Marco Orlandi − *Department of Earth and Environmental Sciences (DISAT), University of Milano−Bicocca, 20126 Milan, Italy;* orcid.org/0000-0002-3787-5834

Luca Zoia − *Department of Earth and Environmental Sciences (DISAT), University of Milano−Bicocca, 20126 Milan, Italy;* orcid.org/0000-0002-0125-6476

Complete contact information is available at: https://pubs.acs.org/10.1021/acssuschemeng.5c12029

Author Contributions

†M.C., F.F., and L.Z.: conceptualization. M.C. and F.F.: investigation. F.F. and M.C.: writing—original draft. M.C., F.F., L.T., S.G., L.G., M.O., and L.Z.: writing—review and editing. L.Z.: supervision. All authors have given approval to the final version of the manuscript. These authors share first authorship.

Funding

The Ph.D. scholarships of M.C. and F.F. have been funded by CORIMAV (Consortium for the Research of Advanced Materials between Pirelli and Milano Bicocca University).

Notes

The authors declare no competing financial interest.

■ REFERENCES

(1) Bontempi, E.; Sorrentino, G. P.; Zanoletti, A.; Alessandri, I.; Depero, L. E.; Caneschi, A. Sustainable Materials and Their Contribution to the Sustainable Development Goals (SDGs): A Critical Review Based on an Italian Example. *Molecules* **2021**, *26* (5), 1407.

(2) Gellerstedt, G. Softwood Kraft Lignin: Raw Material for the Future. *Ind. Crops Prod.* **2015**, *77*, 845−854.

(3) Barana, D.; Ali, S. D.; Salanti, A.; Orlandi, M.; Castellani, L.; Hanel, T.; Zoia, L. Influence of Lignin Features on Thermal Stability and Mechanical Properties of Natural Rubber Compounds. *ACS Sustain. Chem. Eng.* **2016**, *4* (10), 5258−5267.
(4) Nair, S. S.; Sharma, S.; Pu, Y.; Sun, Q.; Pan, S.; Zhu, J. Y.; Deng, Y.; Ragauskas, A. J. High Shear Homogenization of Lignin to Nanolignin and Thermal Stability of Nanolignin-Polyvinyl Alcohol Blends. *ChemSusChem* **2014**, *7* (12), 3513−3520.
(5) Kovačević, V.; Leskovac, M.; Lučić Blagojević, S. Complex Adhesion Effects of Inorganic Nanofillers vs Microfillers in Polymer Composites. *Macromol. Symp.* **2005**, *221* (1), 11−22.
(6) Ago, M.; Huan, S.; Borghei, M.; Raula, J.; Kauppinen, E. I.; Rojas, O. J. High-Throughput Synthesis of Lignin Particles (∼30 Nm to ∼ 2 Mm) via Aerosol Flow Reactor: Size Fractionation and Utilization in Pickering Emulsions. *ACS Appl. Mater. Interfaces* **2016**, *8* (35), 23302−23310.
(7) Chauhan, P. S. Lignin Nanoparticles: Eco-Friendly and Versatile Tool for New Era. *Bioresour. Technol. Rep.* **2020**, *9*, No. 100374.
(8) Garcia Gonzalez, M. N.; Levi, M.; Turri, S.; Griffini, G. Lignin Nanoparticles by Ultrasonication and Their Incorporation in Waterborne Polymer Nanocomposites: ARTICLE. *J. Appl. Polym. Sci.* **2017**, *134* (38), No. 45318.
(9) Sipponen, M. H.; Lange, H.; Crestini, C.; Henn, A.; Österberg, M. Lignin for Nano- and Microscaled Carrier Systems: Applications, Trends, and Challenges. *ChemSusChem* **2019**, *12* (10), 2039−2054.
(10) Xiong, F.; Han, Y.; Wang, S.; Li, G.; Qin, T.; Chen, Y.; Chu, F. Preparation and Formation Mechanism of Size-Controlled Lignin Nanospheres by Self-Assembly. *Ind. Crops Prod.* **2017**, *100*, 146−152.
(11) Zou, T.; Sipponen, M. H.; Henn, A.; Österberg, M. Solvent-Resistant Lignin-Epoxy Hybrid Nanoparticles for Covalent Surface Modification and High-Strength Particulate Adhesives. *ACS Nano* **2021**, *15* (3), 4811−4823.
(12) Lievonen, M.; Valle-Delgado, J. J.; Mattinen, M.-L.; Hult, E.-L.; Lintinen, K.; Kostiainen, M. A.; Paananen, A.; Szilvay, G. R.; Setälä, H.; Österberg, M. A Simple Process for Lignin Nanoparticle Preparation. *Green Chem.* **2016**, *18* (5), 1416−1422.
(13) Collins, M. N.; Nechifor, M.; Tanasă, F.; Zănoagă, M.; McLoughlin, A.; Stróżyk, M. A.; Culebras, M.; Teacă, C.-A. Valorization of Lignin in Polymer and Composite Systems for Advanced Engineering Applications − A Review. *Int. J. Biol. Macromol.* **2019**, *131*, 828−849.
(14) Barana, D.; Orlandi, M.; Zoia, L.; Castellani, L.; Hanel, T.; Bolck, C.; Gosselink, R. Lignin Based Functional Additives for Natural Rubber. *ACS Sustain. Chem. Eng.* **2018**, *6* (9), 11843−11852.
(15) Ferruti, F.; Carnevale, M.; Giannini, L.; Guerra, S.; Tadiello, L.; Orlandi, M.; Zoia, L. Mechanochemical Methacrylation of Lignin for Biobased Reinforcing Filler in Rubber Compounds. *ACS Sustain. Chem. Eng.* **2024**, *12* (37), 14028−14037.
(16) Kaewsakul, W.; Sahakaro, K.; Dierkes, W. K.; Noordermeer, J. W. M. Mechanistic Aspects of Silane Coupling Agents with Different Functionalities on Reinforcement of Silica-Filled Natural Rubber Compounds. *Polym. Eng. Sci.* **2015**, *55* (4), 836−842.
(17) Fortman, D. J.; Snyder, R. L.; Sheppard, D. T.; Dichtel, W. R. Rapidly Reprocessable Cross-Linked Polyhydroxyurethanes Based on Disulfide Exchange. *ACS Macro Lett.* **2018**, *7* (10), 1226−1231.
(18) Seo, M.; Lee, C.; Kim, D.; Ahn, B.; Lee, G.-R.; Kim, W.; Li, S. Saccharide-Containing Conjugates as Eco-Friendly Coupling Agents for Silica Reinforced Rubber Compounds. *Polym. Test.* **2021**, *104*, No. 107379.
(19) Zou, T.; Nonappa, N.; Khavani, M.; Vuorte, M.; Penttilä, P.; Zitting, A.; Valle-Delgado, J. J.; Elert, A. M.; Silbernagl, D.; Balakshin, M.; Sammalkorpi, M.; Österberg, M. Experimental and Simulation Study of the Solvent Effects on the Intrinsic Properties of Spherical Lignin Nanoparticles. *J. Phys. Chem. B* **2021**, *125* (44), 12315−12328.
(20) Ma, Y.; Liao, Y.; Jiang, Z.; Sun, Q.; Guo, X.; Zhang, W.; Hu, C.; Luque, R.; Shi, B.; Sels, B. F. Solvent Effect on the Production of Spherical Lignin Nanoparticles. *Green Chem.* **2023**, *25* (3), 993−1003.
(21) Manisekaran, A.; Grysan, P.; Duez, B.; Schmidt, D. F.; Lenoble, D.; Thomann, J.-S. Solvents Drive Self-Assembly Mechanisms and Inherent Properties of Kraft Lignin Nanoparticles (<50 Nm). *J. Colloid Interface Sci.* **2022**, *626*, 178−192.
(22) Capello, C.; Fischer, U.; Hungerbühler, K. What Is a Green Solvent? A Comprehensive Framework for the Environmental Assessment of Solvents. *Green Chem.* **2007**, *9* (9), 927.
(23) Sipponen, M. H.; Liu, L. Advances in Preparation and Applications of Lignin Nanoparticles. *Lignin Chemistry*; John Wiley & Sons, Ltd., 2024; pp 369−400. DOI: 10.1002/9783527839865.ch13.
(24) Zwilling, J. D.; Jiang, X.; Zambrano, F.; Venditti, R. A.; Jameel, H.; Velev, O. D.; Rojas, O. J.; Gonzalez, R. Understanding Lignin Micro- and Nanoparticle Nucleation and Growth in Aqueous Suspensions by Solvent Fractionation. *Green Chem.* **2021**, *23* (2), 1001−1012.
(25) Ragnar, M.; Lindgren, C. T.; Nilvebrant, N.-O. pKa-Values of Guaiacyl and Syringyl Phenols Related to Lignin. *J. Wood Chem. Technol.* **2000**, *20* (3), 277−305.
(26) Thannhauser, T. W.; Konishi, Y.; Scheraga, H. A. Analysis for Disulfide Bonds in Peptides and Proteins. *Methods in Enzymology*; Sulfur and Sulfur Amino Acids; Academic Press, 1987; Vol. *143*, pp 115−119. DOI: 10.1016/0076-6879(87)43020-6.
(27) Tadiello, L.; Giannini, L.; Wuthicharn, C.; Wuthicharn, C. Tyre for Vehicle Wheels. Patent WO2022144759A1, July 7, 2022. https://patents.google.com/patent/WO2022144759A1/en (accessed 2022-09-12).
(28) Heinrich, G.; Klüppel, M.; Vilgis, T. A. Reinforcement of Elastomers. *Curr. Opin. Solid State Mater. Sci.* **2002**, *6* (3), 195−203.
(29) Israelachvili, J. N. *Intermolecular and Surface Forces*; Academic Press, 2011.
(30) Stöckelhuber, K. W.; Das, A.; Jurk, R.; Heinrich, G. Contribution of Physico-Chemical Properties of Interfaces on Dispersibility, Adhesion and Flocculation of Filler Particles in Rubber. *Polymer* **2010**, *51* (9), 1954−1963.
(31) Amrollahi, A.; Razzaghi-Kashani, M.; Hosseini, S. M.; Habibi, N. Carbon Black/Silica Hybrid Filler Networking and Its Synergistic Effects on the Performance of Styrene-Butadiene Rubber Composites. *Polym. J.* **2022**, *54* (7), 931−942.
(32) Carretier, V.; Pucci, M. F.; Lacoste, C.; Regazzi, A.; Lopez-Cuesta, J. M. Surface Energy Determination of Particles Used as Fillers in Polymers: Application to Lignin/PLA Composites; EPFL, 2022; DOI: 10.5075/epfl.
(33) Suzuki, M.; Kondor, A.; Sakuraba, Y.; Rojas, O. J.; Ago, M. Surface Energy Properties of Lignin Particles Studied by Inverse Gas Chromatography and Interfacial Adhesion in Polyester Composites with Electromagnetic Transparency. *Cellulose* **2022**, *29* (5), 2961−2973.
(34) Heideman, G.; Datta, R. N.; Noordermeer, J. W. M.; van Baarle, B. Activators in Accelerated Sulfur Vulcanization. *Rubber Chem. Technol.* **2004**, *77* (3), 512−541.
(35) Hosseini, S. M.; Torbati-Fard, N.; Kiyani, H.; Razzaghi-Kashani, M. Comparative Role of Interface in Reinforcing Mechanisms of Nano Silica Modified by Silanes and Liquid Rubber in SBR Composites. *J. Polym. Res.* **2016**, *23* (9), 1−10.
(36) Stöckelhuber, K. W.; Svistkov, A. S.; Pelevin, A. G.; Heinrich, G. Impact of Filler Surface Modification on Large Scale Mechanics of Styrene Butadiene/Silica Rubber Composites. *Macromolecules* **2011**, *44* (11), 4366−4381.
(37) Liu, R.; Li, J.; Lu, T.; Han, X.; Yan, Z.; Zhao, S.; Wang, H. Comparative Study on the Synergistic Reinforcement of Lignin between Carbon Black/Lignin and Silica/Lignin Hybrid Filled Natural Rubber Composites. *Ind. Crops Prod.* **2022**, *187*, No. 115378.
(38) Fröhlich, J.; Niedermeier, W.; Luginsland, H.-D. The Effect of Filler−Filler and Filler−Elastomer Interaction on Rubber Reinforcement. *Compos. Part Appl. Sci. Manuf.* **2005**, *36* (4), 449−460.
(39) Kaewsikoun, S.; Kumarn, S.; Sakdapipanich, J. The Effect of Non-Rubber Components on Mechanical Properties of TESPD Silane Coupling Agent in Silica-Filled Rubber Compounds. *IOP Conf. Ser. Mater. Sci. Eng.* **2020**, *773* (1), No. 012029.

(40) Shakun, A.; Sarlin, E.; Vuorinen, J. Material-Related Losses of Natural Rubber Composites with Surface-Modified Nanodiamonds. *J. Appl. Polym. Sci.* **2020**, *137* (18), No. 48629.

https://doi.org/10.1021/acssuschemeng.5c12029
ACS Sustainable Chem. Eng. XXXX, XXX, XXX−XXX